Chin. Phys. Lett. **39**, 057401 (2022) **Express Letter**

Effect of Impurity on the Doping-Induced in-Gap States in a Mott Insulator

Cheng-Ping He(贺诚平)[1], Shun-Li Yu(于顺利)[1,2], Tao Xiang(向涛)[3,4,5*], and Jian-Xin Li(李建新)[1,2*]

[1]*National Laboratory of Solid State Microstructures and School of Physics, Nanjing University, Nanjing 210093, China*
[2]*Collaborative Innovation Center of Advanced Microstructures, Nanjing University, Nanjing 210093, China*
[3]*Institute of Physics, National Laboratory for Condensed Matter Physics, Chinese Academy of Sciences, Beijing 100190, China*
[4]*Department of Physics, University of Chinese Academy of Sciences, Beijing 100190, China*
[5]*Beijing Academy of Quantum Information Sciences, Beijing 100193, China*

(Received 5 April 2022; accepted 20 April 2022; published online 27 April 2022)

Motivated by the recent measurements of the spatial distribution of single particle excitation states in a hole-doped Mott insulator, we study the effects of impurity on the in-gap states, induced by the doped holes, in the Hubbard model on the square lattice by the cluster perturbation theory. We find that a repulsive impurity potential can move the in-gap state from the lower Hubbard band towards the upper Hubbard band, providing a good account for the experimental observation. The distribution of the spectral function in the momentum space can be used to discriminate the in-gap state induced by doped holes and that by the impurity. The spatial characters of the in-gap states in the presence of two impurities are also discussed and compared to the experiment.

DOI: 10.1088/0256-307X/39/5/057401

The parent compounds of high-T_c superconducting cuprates are Mott insulators with antiferromagnetic long-range orders in the CuO_2 layers. High temperature superconductivity is realized by doping holes or electrons to these parent compounds. A thorough investigation of doped Mott insulators is crucial to the understanding of high-T_c mechanism in cuprates.[1−4] In the past decades, great efforts have been devoted to this kind of studies, both experimentally[5−18] and theoretically.[19−32]

A characteristic feature of a doped Mott insulator is the emergence of the in-gap states in the single-particle spectra inside the Mott gap. Upon one hole or electron doping, there is a spectral weight transfer from the upper Hubbard band (UHB) and the lower Hubbard band (LHB),[19] in association with the emerged in-gap state. With increasing doping, the in-gap states smear extensively inside the Mott gap, and eventually drive the insulator-metal transition.[6,17,18] This is a feature not observed in conventional band insulators, in which doping will only shift the level of the chemical potential. Therefore, the in-gap states are a clear manifestation of the strong correlation effects between electrons in the Mott insulator. A number of theoretical pictures have been proposed to reveal the origin of the in-gap states. These include the relaxation effect of the binding energy between doublon and holon by doping,[22,27] the hybridization between cofermions and quasiparticles which are constructed by doublon operators,[28,29] and the coupling of the emergent states with antiferromagnetic correlations[21] or magnetic excitations.[31,32]

Experimentally, the in-gap states were observed in the local density of states (LDOS) measurements by high-resolution scanning tunneling microscopy (STM) on $Ca_2CuO_2Cl_2$ with a Cl defect.[5,6] A Cl atom substitutes an O atom, and acts as a single electron dopant as well as an impurity. The in-gap states induced by the Cl defect are observed close to the chemical potential below UHB, and their LDOS exhibits a systematic evolution measured at different lattice sites. The key features of the in-gap states could be reproduced by numerical calculations based on the cluster perturbation theory[33] and the variational Monte Carlo simulations.[34] More recently, the LDOS in $Ca_2CuO_2Cl_2$ with a Ca vacancy is measured by STM.[7] Similar to the system with a Cl defect, the in-gap states were also found to localize around the Ca vacancy and vary at different sites. As the Ca-vacancy acts as a hole dopant, the in-gap state is expected to lie near LHB .[19] However, the experiment shows that the in-gap states are still close to UHB, and at nearly the same energy inside the Mott gap when measured at several different sites in the vicinity of the Ca vacancy. In the presence of two Ca vacancies, the spatial distribution of LDOS varies dramatically with the relative distance of the two vacancies. Particularly, the in-gap state moves to a lower energy and its spectrum exhibits a two-peak structure at the sites along the direction perpendicular to the line connecting the two vacancies.

Motivated by the STM measurement results,[7] we

*Corresponding authors. Email: txiang@iphy.ac.cn; jxli@nju.edu.cn
© 2022 Chinese Physical Society and IOP Publishing Ltd

study the effect of impurity on the in-gap state in the hole doped Hubbard model on the two-dimensional (2D) square lattice using the cluster perturbation theory (CPT).[35,36] We find that an impurity potential can move the doping-induced in-gap state from LHB towards UHB, in consistence with the STM observation in $Ca_2CuO_2Cl_2$ with a Ca vacancy.[7] In the case two vacancies are present, the spatial distributions of the in-gap states also exhibit two features similar to those observed by the experiment.[7] In the momentum (k) space, the contributions of the doping-induced state differs from the impurity-induced state in their distributions. This allows us to show that the doping-induced state situates around the corner of the Brillouin zone (BZ). Comparing the spectral function of the in-gap state with that of the one-dimensional (1D) Hubbard model, we suggest that the 2D in-gap state is related to the spinon-antiholon continuum in the 1D Hubbard model.

The Hubbard model reads

$$H = -t\sum_{\langle i,j\rangle\sigma}(c^{\dagger}_{i,\sigma}c_{j,\sigma}+\text{h.c.}) + U\sum_{i} n_{i,\downarrow}n_{i,\uparrow} - \mu\sum_{i,\sigma} n_{i,\sigma} + \mu_{\text{s}}n_{\text{s}}, \quad (1)$$

where μ_{s} is the impurity potential at one site and the other notations are standard. The CPT is an approximation method based on the exact diagonalization of finite clusters.[35–42] It treats the intercluster coupling as a perturbation. The CPT method and the evaluation of the single-particle spectral function and LDOS are introduced in the Supplementary Material. In the discussion below, we take $U/t = 10$ and the broadening factor $\eta/t = 0.24$. The whole system consists of 6×6 clusters in the 2D calculation and 20 clusters in the 1D one, respectively.

Spectrum in the Absence of Impurity. We start with the system without impurity. LDOSs as a function of energy at different lattice sites are shown in Fig. 1, in which the solid lines correspond to the results at the sites with same colors denoted in the inset. Figure 1(a) shows the results at half filling with the tiling of a 16-site cluster, which is the largest cluster with the C_4 rotational symmetry we can handle. LDOSs at the sites with the same color in the cluster are identical because of symmetry. The difference in LDOSs between different color sites is due to the approximation used in the CPT where the intra- and intercluster hoppings are treated differently. The difference manifests itself mainly in the peak heights of the spectrum. The general feature of Fig. 1(a) is the existence of the Mott gap with symmetric UHB and LHB. When one hole is doped into the system, the in-gap states emerge just above the LHB as shown in Fig. 1(b). The spectral weights of the in-gap states contribute mainly from UHB, as can be seen from a comparison with the spectral function at half filling denoted by the gray dashed line. The results are consistent with our early CPT calculations.[33] We also check the results with different sizes and shapes of clusters, as presented in Figs. 1(c)–1(e). It shows the stability of the in-gap states and the general feature of the spectral weight transfers.

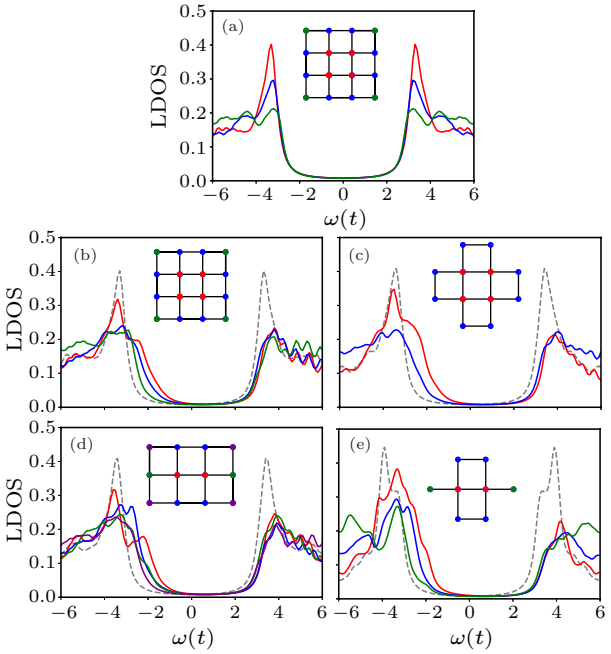

Fig. 1. (a) LDOSs calculated with the tiling of a 16-site cluster without doping. (b)–(e) LDOSs for one-hole doping calculated with tilings of different cluster sizes and/or shapes shown in the inset. The solid lines with different colors represent the results at the lattice sites with the same colors denoted in the inset. The grey dashed lines in (b)–(e) denote the result at the red lattice site without doping.

In the $U/t \to \infty$ limit, LHB is fully filled while UHB is completely empty at half filling, because they represent the possibility of singly occupied states and that of doubly-occupied states, respectively. When a hole is doped into the system, it eliminates simultaneously one singly occupied state and one channel to add an electron to a site that is already occupied. Thus, the spectral weight of both LHB and UHB decreases by 1, and the missing spectral weights are transferred to the in-gap state. In a finite U system, the double occupancy is finite,[33] the transferred spectral weights come mainly from the UHB as can be clearly seen in Figs. 1(b)–1(e). This feature is consistent with the experiment.[7] However, the in-gap state appears near the top of LHB in the hole doping [the peak or hump in the red line in Figs. 1(b)–(d)], which does not agree with the experimental observation in $Ca_2CuO_2Cl_2$ with a Ca-vacancy, where the in-gap state is below UHB.[7]

Effects of Impurity Potential. In Fig. 2, we show LDOSs at different lattice sites with one hole and a repulsive impurity potential μ_{s} at the site labeled by the red cross in Fig. 2(a). The general features are: (i)

the size of the Mott gap is not affected by the impurity site, except at the impurity site [Fig. 2(b)]. We note that, in the experiment,[7] the cleaved surface is the Cl layer with Cl lying directly above the Cu sites in the CuO_2 plane and the Ca vacancy is at the center of four Cl atoms. Therefore, the LDOS calculated at the impurity site is expected to overestimate the impurity effects. (ii) The position of the in-gap states moves away from LHB towards UHB as the value of μ_s increases. (iii) The spectral weight of the in-gap states decreases gradually with the distance away from the impurity, however the energy scale does not vary with the lattice sites. These features are consistent with the STM experimental observations in $Ca_2CuO_2Cl_2$ with a single Ca vacancy.[7]

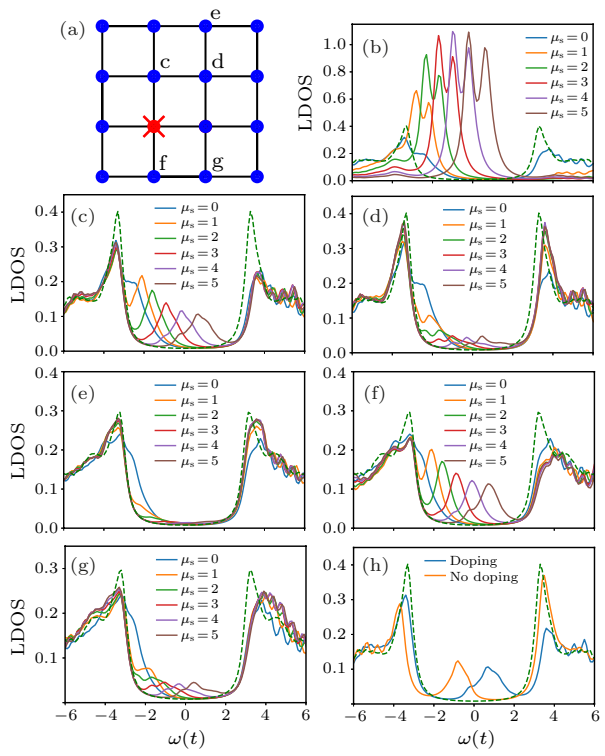

Fig. 2. (a) A 16-site cluster with an impurity in the red cross site. (b) LDOS at the impurity site for different impurity potentials μ_s with one-hole doping. (c)–(g) LDOSs at the site c, d, e, f, and g denoted in the cluster for different μ_s with one-hole doping. (h) A comparison of LDOS for $\mu_s = 5$ between the one-hole doping and no doping case.

An impurity may also induce an impurity state inside the Mott gap. Such an impurity-induced state has indeed been found inside the Mott gap for the Hubbard model at half filling as seen in Fig. 2(h). However, there is no systematic spectral weight transfers from UHB, and it looks similar to the impurity-induced state in conventional energy-band insulators. The interesting phenomenon we observed is that LDOSs of the in-gap states show a main peak upon the introduction of the impurity, though the in-gap state already exists. Inspecting the results [Figs. 2(c)–2(g)], we find that a spectral shoulder becomes more pronounced when $\mu_s \geq 3$. Considering that the impurity does not cause a noticeable spectral weight transfer and its induced state is at a relative high energy, we suggest that the hybridization between the doping-induced in-gap state and impurity-induced state pushes the in-gap state towards UHB, and leads to the feature consisting with the experimental observation.[7]

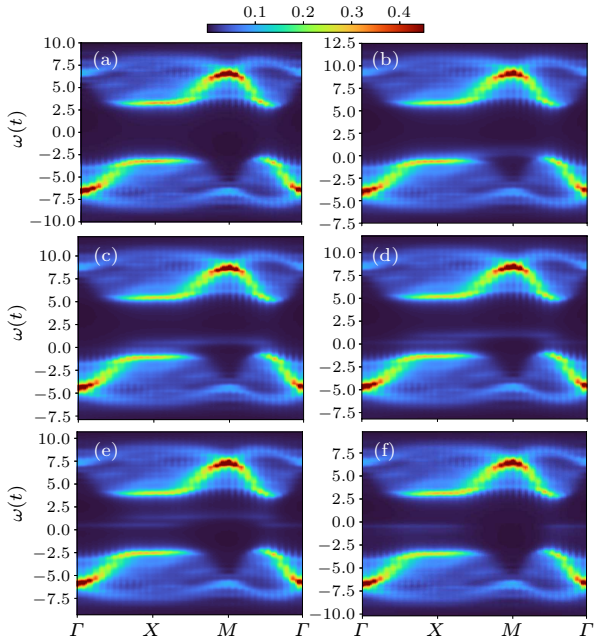

Fig. 3. Spectral function of the 2D Hubbard model calculated by CPT: (a) at half filling, (b)–(e) at doping $\delta \approx 0.016$ with $\mu_s = 0, 2, 3, 5$, respectively, (f) at half filling and $\mu_s = 5$.

Then, we go to study the evolution of in-gap states in the momentum space. Figure 3(a) shows the single-particle spectral function of the 2-D Hubbard model at half filling, which exhibits a Mott gap between LHB and UHB. The results for a hole doping concentration $\delta \approx 0.016$ in a 6×6 tiling of a 16-site cluster are shown in Fig. 3(b). One can see that the additional state induced by doping appears in the region from the $X = (0, \pi)$ point to the midpoint of the $M = (\pi, \pi)$ to Γ line, along the high symmetric Γ–X–M–Γ direction. However, in the Γ–X and Γ–M directions, it merges into the edge of the LHB , preventing us to distinguish it from the LHB . After introducing the impurity, the energy of the additional state increases and moves towards the UHB [Figs. 3(c)–3(e)], which is consistent with the behavior of LDOSs in the real space discussed above. At the meantime, the spectrum of the additional state is split into two branches, reflecting the hybridization between the doping-induced state and impurity-induced state. Interestingly, though these two branches exhibit similar flat dispersions, they show striking difference in their distribution in the k space. Namely, in the Γ–X–M–Γ direction, the upper branch stretches from the midpoint of the Γ–X line to the midpoint of the M–Γ line, while the lower branch breaks into two sec-

tors with one along the Γ point to the midpoint of the X–M line and the other from the midpoint of the M–Γ line to the Γ point. To identify the main characters of the two branches, we present the result without hole doping but with an impurity in Fig. 3(f). It shows clearly that the lower branch contributes mainly from the impurity-induced state. Thus, the doping-induced in-gap states localize around the M region in the BZ. One point we would like to note is that the whole energy band shifts downwards when the impurity term is added as shown in Figs. 3(c)–3(e). This is due to the fact that the impurity will drag a small number of incoherent spectral weights into the Mott gap, in the process of moving the in-gap state. These spectral weights lift upwards the Fermi energy, though they are hard to be noticed compared to the in-gap state.

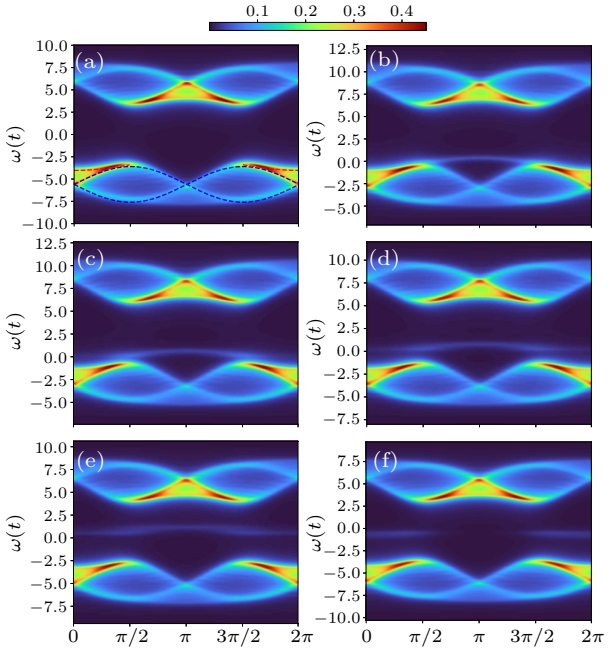

Fig. 4. Spectral function of the 1D Hubbard model calculated by the CPT with the 20×1 tiling of a 14-site cluster: (a) at half filling, (b)–(e) at hole doping $\delta \approx 0.018$ with $\mu_{\rm s} = 0, 2, 3, 5$, respectively, (f) at half filling and $\mu_{\rm s} = 5$.

As the one-dimensional (1D) Hubbard model without impurity can be understood exactly,[43] we wish to deepen our understanding by making a comparison with the 1D Hubbard model. First, we note that LDOS in the Hubbard chain with one hole doping and an impurity exhibit quite similar features as in the 2D Hubbard model [see the Supplementary Material]. Figure 4(a) presents $A(\omega, \boldsymbol{k})$ at half filling, which shows two distinct dispersive features both in LHB and UHB. Considering the hole-doping case, we focus on the LHB. The two features can be identified as the spinon and holon excitations,[25,26,44] indicated by the red and blue dashed lines, respectively. Because of the spin-charge separation, the electron excitation satisfies the momentum and energy conservation relations $k = k_{\rm s} - k_{\rm h}$ and $\omega(k) = E_{\rm s}(k_{\rm s}) - E_{\rm h}(k_{\rm h})$,[44–48] with $k_{\rm s/h}$ and $E_{\rm s/h}(k_{\rm s/h})$ representing the spinon/holon momentum and energy. According to the Bethe ansatz solution,[26,44] the spinon and holon momenta situate at $|k_{\rm s}| \leq k_{\rm F}$ and $|k_{\rm h}| \leq 2k_{\rm F}$, with the Fermi wave vector $k_{\rm F} = \pi(1-\delta)/2$ and δ the doping concentration. The red dashed line ($\propto -\cos k$) is for the case of a fixed $k_{\rm h} = 0$ and the blue dashed line ($\propto \pm \sin k$) a fixed $|k_{\rm s}| = k_{\rm F}$, so they follow the spinon and holon dispersions, respectively. The result at a hole doping $\delta \approx 0.018$ for the 20×1 tiling of a 14-site cluster, is shown in Fig. 4(b), which agrees well with the density matrix renormalization group calculations.[25,26,44,47] The hole doping induces additional electronic states above the Fermi level ($E_{\rm F}$), which go into the Mott gap to form the in-gap state and extend from $\pi/2$ to $3\pi/2$ [Fig. 4(b)]. Upon hole doping, antiholons emerge in the region $2k_{\rm F} < |k_{h^*}| < \pi$ as $k_{\rm F}$ is not at $\pi/2$, and the spinon-antiholon continuum with excitation energy $-\omega(k)$ constitutes the in-gap states above $E_{\rm F}$. The introduction of an impurity moves the additional states away from LHB towards UHB, and they exhibit themselves in the whole BZ. At a large $\mu_{\rm s}$, such as $\mu_{\rm s} = 5$ shown in Fig. 4(e), a split of the in-gap state can be differentiated clearly, and the upper branch distributes mainly in the region of $\pi/2$ to $3\pi/2$, while the lower branch mainly in the regions of 0 to $\pi/2$ and $3\pi/2$ to π. With a comparison to the non-doping case shown in Fig. 4(f), we can attribute the upper branch essentially to the doping-induced in-gap state. These findings suggest that the 1D Hubbard model behaves similarly as in the 2D case. Thus, in addition to the localization in the real space, the doping induced in-gap state appears only in a limited momentum domain around the corners (ends in 1D) of the BZ, and that in the 2D system is related to the spinon-antiholon continuum.

Effects of Two Impurities. Figure 5 shows the CPT results of LDOS in the 2D Hubbard model with two impurities situating at the lattice sites denoted by the red crosses and the impurity potential $\mu_{\rm s} = 5$, where two different spatial distributions of the impurities in the cluster are presented in Figs. 5(a) and 5(b). A general feature is that the in-gap states move towards the UHB with the increase of the impurity potential, which is similar to the one-impurity case. However, regardless of the symmetric or non-symmetric distributions of impurities [Figs. 5(a) and 5(b)], LDOS exhibits a two-peak structure at the sites along the direction perpendicular to the line connecting the two impurities, such as the sites labeled as 6 and 3 in Fig. 5(a), and 10 and 6 in Fig. 5(b). It results from the interference of the two impurities. Besides the lattice sites along the perpendicular direction, the in-gap state at all other sites exhibits an one-peak structure and its spectral weight decreases with the distance deviating from the impurities. Moreover, compared to the energy position of the in-gap state in the one-impurity case as replotted here by the dashed

color lines, the LDOS at these sites now moves to a lower energy. These spatial characters for LDOS of the in-gap states are consistent with those observed in the STM measurement for $Ca_2CuO_2Cl_2$.[7]

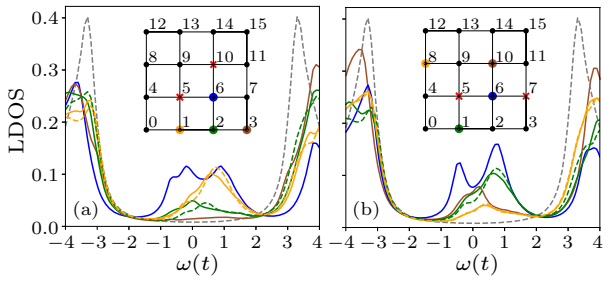

Fig. 5. LDOSs at different lattice sites for two impurities with $\mu_s = 5$, as denoted by the red crosses in the inset. Here (a) and (b) represent two typical spatial distributions of two impurities. The colored lines are the results at the sites with the same colors. The gray dashed line denotes the result at sites numbered 5 and its symmetric sites 6, 9, 10 at half filling and without impurity. The other colored dashed lines are the results in the one-impurity case reproduced from Fig. 3 to make a comparison.

In summary, we have studied the effects of impurity on the doping-induced in-gap states in the Hubbard model by the cluster perturbation theory. Our results show that the impurity with a repulsive potential can move the in-gap states in a hole doped system from the lower Hubbard band towards the upper Hubbard band, which provides an explanation to the experimental observation in $Ca_2CuO_2Cl_2$ with a Ca vacancy.[7] When there exist two impurities, the obtained characteristic spatial distributions for the local density of states of the in-gap states are also consistent with the experimental observation. From the spectral functions of the single-particle excitations, we discriminate clearly the contributions from the doping-induced state and the impurity-induced state due to their different distributions in the momentum space and show that the doping-induced states situate around the corner of the Brillouin zone. We suggest that the in-gap state induced by doping is related to the spinon-antiholon continuum in the one-dimensional Hubbard model.

Acknowledgements. This work was supported by the National Key Research and Development Program of China (Grant Nos. 2017YFA0302901 and 2021YFA1400400), and the National Natural Science Foundation of China (Grant Nos. 11888101, 12074175, and 92165205).

References

[1] Bednorz J G and Müller K A 1986 *Z. Phys. B-Condens. Matter* **64** 189
[2] Lee P A, Nagaosa N and Wen X G 2006 *Rev. Mod. Phys.* **78** 17
[3] Dagotto E 1994 *Rev. Mod. Phys.* **66** 763
[4] Imada M, Fujimori A and Tokura Y 1998 *Rev. Mod. Phys.* **70** 1039
[5] Ye C, Cai P, Yu R, Zhou X, Ruan W, Liu Q, Jin C and Wang Y 2013 *Nat. Commun.* **4** 1365
[6] Cai P, Ruan W, Peng Y, Ye C, Li X, Hao Z, Zhou X, Lee D H and Wang Y 2016 *Nat. Phys.* **12** 1047
[7] Li H, Ye S, Zhao J, Jin C and Wang Y 2021 *Sci. Bull.* **66** 1395
[8] Sun Z, Guevara J M, Sykora S, Pärschke E M, Manna K, Maljuk A, Wurmehl S, van den Brink J, Büchner B and Hess C 2021 *Phys. Rev. Res.* **3** 023075
[9] Wang Y, He Y, Wohlfeld K *et al.* 2020 *Commun. Phys.* **3** 1
[10] Chen Z, Wang Y, Rebec S N, Jia T, Hashimoto M, Lu D, Moritz B, Moore R G, Devereaux T P and Shen Z X 2021 *Science* **373** 1235
[11] Ronning F, Shen K M, Armitage N P, Damascelli A, Lu D H, Shen Z X, Miller L L and Kim C 2005 *Phys. Rev. B* **71** 094518
[12] Meevasana W, Zhou X, Sahrakorpi S *et al.* 2007 *Phys. Rev. B* **75** 174506
[13] Valla T, Kidd T, Yin W G, Gu G, Johnson P, Pan Z H and Fedorov A 2007 *Phys. Rev. Lett.* **98** 167003
[14] Graf J, Gweon G H, McElroy K *et al.* 2007 *Phys. Rev. Lett.* **98** 067004
[15] He Y, Hashimoto M, Song D *et al.* 2018 *Science* **362** 62
[16] Chen S D, Hashimoto M, He Y *et al.* 2019 *Science* **366** 1099
[17] Hu C, Zhao J, Gao Q *et al.* 2021 *Nat. Commun.* **12** 1
[18] Gao Q, Zhao L, Hu C *et al.* 2020 *Chin. Phys. Lett.* **37** 087402
[19] Eskes H, Meinders M B J and Sawatzky G A 1991 *Phys. Rev. Lett.* **67** 1035
[20] Dagotto E, Ortolani F and Scalapino D 1992 *Phys. Rev. B* **46** 3183
[21] Preuss R, Hanke W and von der Linden W 1995 *Phys. Rev. Lett.* **75** 1344
[22] Phillips P, Choy T P and Leigh R G 2009 *Rep. Prog. Phys.* **72** 036501
[23] Phillips P 2010 *Rev. Mod. Phys.* **82** 1719
[24] Eder R, Seki K and Ohta Y 2011 *Phys. Rev. B* **83** 205137
[25] Kohno M 2018 *Rep. Prog. Phys.* **81** 042501
[26] Kohno M 2010 *Phys. Rev. Lett.* **105** 106402
[27] Sakai S, Motome Y and Imada M 2009 *Phys. Rev. Lett.* **102** 056404
[28] Yamaji Y and Imada M 2011 *Phys. Rev. Lett.* **106** 016404
[29] Yamaji Y and Imada M 2011 *Phys. Rev. B* **83** 214522
[30] Kang J, Yu S L, Xiang T and Li J X 2011 *Phys. Rev. B* **84** 064520
[31] Kohno M 2012 *Phys. Rev. Lett.* **108** 076401
[32] Kohno M 2015 *Phys. Rev. B* **92** 085129
[33] Leong W H, Yu S L, Xiang T and Li J X 2014 *Phys. Rev. B* **90** 245102
[34] Wu H K and Lee T K 2017 *Phys. Rev. B* **95** 035133
[35] Sénéchal D, Perez D and Pioro-Ladrière M 2000 *Phys. Rev. Lett.* **84** 522
[36] Sénéchal D, Perez D and Plouffe D 2002 *Phys. Rev. B* **66** 075129
[37] Pairault S, Sénéchal D and Tremblay A M S 1998 *Phys. Rev. Lett.* **80** 5389
[38] Zacher M G, Eder R, Arrigoni E and Hanke W 2000 *Phys. Rev. Lett.* **85** 2585
[39] Sénéchal D and Tremblay A M S 2004 *Phys. Rev. Lett.* **92** 126401
[40] Yu S L, Xie X C and Li J X 2011 *Phys. Rev. Lett.* **107** 010401
[41] Yu S L and Li J X 2012 *Phys. Rev. B* **85** 144402
[42] Potthoff M, Aichhorn M and Dahnken C 2003 *Phys. Rev. Lett.* **91** 206402
[43] Lieb E H and Wu F Y 1968 *Phys. Rev. Lett.* **20** 1445
[44] Benthien H, Gebhard F and Jeckelmann E 2004 *Phys. Rev. Lett.* **92** 256401
[45] Suzuura H and Nagaosa N 1997 *Phys. Rev. B* **56** 3548
[46] Xiang T and d'Ambrumenil N 1992 *Phys. Rev. B* **45** 8150
[47] Nocera A, Essler F H L and Feiguin A E 2018 *Phys. Rev. B* **97** 045146
[48] Kumar U, Nocera A, Price G, Stiwinter K, Johnston S and Datta T 2020 *Phys. Rev. B* **102** 075134

Supplemental Material: Effect of impurity on the doping-induced in-gap states in a Mott insulator

Cheng-Ping He,[1] Shun-Li Yu,[1,2] Tao Xiang,[3,4,5,*] and Jian-Xin Li[1,2,†]

[1]*National Laboratory of Solid State Microstructures and School of Physics, Nanjing University, Nanjing 210093, China*
[2]*Collaborative Innovation Center of Advanced Microstructures, Nanjing University, Nanjing 210093, China*
[3]*Institute of Physics, National Laboratory for Condensed Matter Physics, Chinese Academy of Sciences, Beijing,*
[4]*Department of Physics, University of Chinese Academy of Sciences, Beijing 100190, China*
[5]*Beijing Academy of Quantum Information Sciences, Beijing 100193, China*

I. CALCULATION METHOD BASED ON THE CLUSTER PERTURBATION THEORY

We use the cluster perturbation theory (CPT) to carry out the calculations. The CPT is an approximation method based on the exact diagonalization of finite clusters and treating the intercluster coupling as a perturbation [1–9]. Hence, it can treat much larger lattice systems than the exact diagonalization, which is important for our detailed spectral analysis. In CPT, the whole system is divided into identical clusters which constitute a superlattice (see Fig. S1), so the Hamiltonian is rewritten as,

$$H = H' + V, \tag{1}$$

where H' is the cluster Hamiltonian obtained by cutting the hopping terms between different clusters, and V contains the inter-cluster hopping terms. In the superlattice, the site i in the original lattice is represented by two new indices (c,α), where c is the index of the cluster and α labels the site in each cluster. By using the Lanczos exact diagonalization technique, the Green's function $\boldsymbol{G}'^{c}$ for the cluster c can be calculated from its definition

$$G'^{c}_{\alpha\sigma,\beta\sigma'}(\omega) = \langle\Omega^c| c^{c}_{\alpha\sigma} \frac{1}{\omega - H'_c + E^c_0 + i\eta} c^{c\dagger}_{\beta\sigma'} |\Omega^c\rangle + \langle\Omega^c| c^{c\dagger}_{\alpha\sigma} \frac{1}{\omega - H'_c - E^c_0 + i\eta} c^{c}_{\beta\sigma'} |\Omega^c\rangle, \tag{2}$$

where E^c_0 is the energy of the ground state $|\Omega^c\rangle$ and η is the Lorentzian broadening. The Green's function $\boldsymbol{G}_{cpt}(\omega)$ for the whole system is calculated from

$$\boldsymbol{G}^{-1}_{cpt}(\omega) = \boldsymbol{G}'^{-1}(\omega) - \boldsymbol{V}. \tag{3}$$

Here, $\boldsymbol{G}_{cpt}(\omega)$, $\boldsymbol{G}'(\omega)$ and $\boldsymbol{V}$ are $2N_s \times 2N_s$ matrices, where $N_s = N_c \times N$ is the number of the whole lattice sites with N_c the number of clusters and N the number of sites in each cluster. In Eq. (3), $\boldsymbol{G}'(\omega)$ and $\boldsymbol{V}$ are defined by

$$G'_{c\alpha\sigma,c'\beta\sigma'}(\omega) = \delta_{cc'} G'^{c}_{\alpha\sigma,\beta\sigma'}(\omega) \tag{4}$$

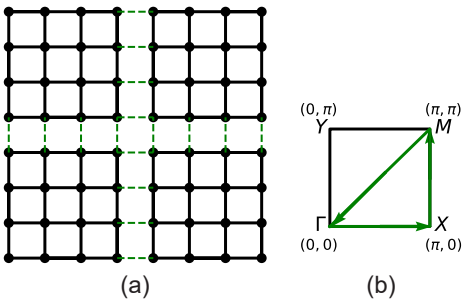

FIG. S1. (Color on line) (a) Tiling of the square lattice with 16-sites, the inter-cluster hopping terms denoted by the green dashed lines are treated as perturbations in CPT. (b) Path in the momentum space along which we present our results for the two-dimensional system in the main text.

and

$$V_{c\alpha\sigma,c'\beta\sigma'} = -t\delta_{c\neq c'}\delta_{\langle c\alpha,c'\beta\rangle}\delta_{\sigma\sigma'}, \tag{5}$$

where $\langle c\alpha, c'\beta\rangle$ means that (c,α) and (c',β) are two inter-cluster nearest-neighbor sites. The local density of states (LDOS) at the site $i = (c,\alpha)$ is given by

$$A_i(\omega) = -\frac{1}{\pi}\sum_{\sigma} \mathrm{Im} G_{cpt,i\sigma,i\sigma}(\omega). \tag{6}$$

In order to obtain the momentum-space spectral function, we transfer $\boldsymbol{V}$ from the real space into the momentum space to get a $2N \times 2N$ matrix $\boldsymbol{V}(\tilde{k})$ with $\tilde{k}$ the momentum in the first Brillouin zone of the superlattice, and the Green's function of the superlattice is given by

$$\boldsymbol{G}^{-1}_{cpt}(\omega,\tilde{\boldsymbol{k}}) = \boldsymbol{G}'^{c-1}(\omega) - \boldsymbol{V}(\tilde{\boldsymbol{k}}). \tag{7}$$

The Green's function of the original lattice can be calculated by a periodization procedure

$$G_{\sigma,\sigma'}(\omega,\boldsymbol{k}) = \frac{1}{N}\sum_{\alpha,\beta}[G_{cpt}]_{\alpha\sigma,\beta\sigma'}(\omega,\boldsymbol{k}) e^{-i\boldsymbol{k}\cdot(\boldsymbol{r}_\alpha - \boldsymbol{r}_\beta)}, \tag{8}$$

where $\boldsymbol{k}$ is the momentum in the original first Brillouin zone.

* txiang@iphy.ac.cn
† jxli@nju.edu.cn

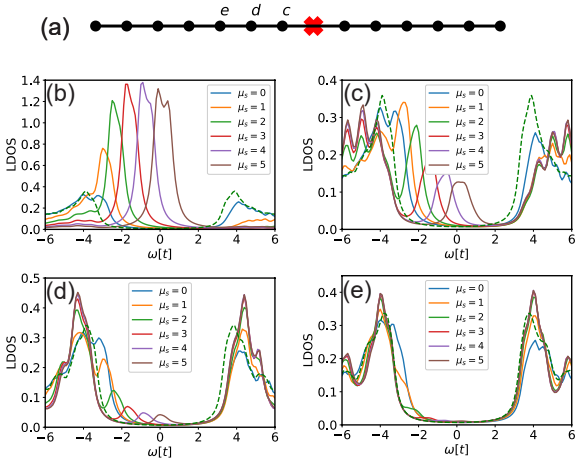

FIG. S2. (a) A 14-site cluster with an impurity at the red cross site. (b)-(e) LDOS at impurity site (b) and the sites with the same labels in (a) for different impurity potential μ_s.

Then, the momentum-space spectral function is given by

$$A(\omega, \boldsymbol{k}) = -\frac{1}{\pi} \sum_{\sigma} \mathrm{Im} G_{\sigma,\sigma}(\omega, \boldsymbol{k}). \tag{9}$$

II. LDOS IN THE ONE-DIMENSIONAL HUBBARD MODEL WITH ONE IMPURITY

In Fig.S2, we show the local density of states of in-gap states in a one-dimensional Hubbard model calculated using the cluster perturbation theory.

[1] D. Sénéchal, D. Perez, and M. Pioro-Ladrière, Phys. Rev. Lett. **84**, 522 (2000).
[2] D. Sénéchal, D. Perez, and D. Plouffe, Phys. Rev. B **66**, 075129 (2002).
[3] S. Pairault, D. Sénéchal, and A.-M. S. Tremblay, Phys. Rev. Lett. **80**, 5389 (1998).
[4] M. G. Zacher, R. Eder, E. Arrigoni, and W. Hanke, Phys. Rev. Lett. **85**, 2585 (2000).
[5] D. Sénéchal and A.-M. S. Tremblay, Phys. Rev. Lett. **92**, 126401 (2004).
[6] J. Kang, S.-L. Yu, T. Xiang, and J.-X. Li, Phys. Rev. B **84**, 064520 (2011).
[7] S.-L. Yu, X. C. Xie, and J.-X. Li, Phys. Rev. Lett. **107**, 010401 (2011).
[8] S.-L. Yu and J.-X. Li, Phys. Rev. B **85**, 144402 (2012).
[9] M. Potthoff, M. Aichhorn, and C. Dahnken, Phys. Rev. Lett. **91**, 206402 (2003).